Petroleum Science 19 (2022) 1382–1389

Contents lists available at ScienceDirect

Petroleum Science

journal homepage: www.keaipublishing.com/en/journals/petroleum-science

Original Paper

N-hydroxyphthalimide anchored on hexagonal boron nitride as a metal-free heterogeneous catalyst for deep oxidative desulfurization

Lin-Jie Lu [a], Pei-Wen Wu [a, *], Jing He [a], Ming-Qing Hua [a], Yan-Hong Chao [b], Ning Yang [a], Lin-Lin Chen [a], Wei Jiang [a], Lei Fan [c], Hong-Bing Ji [d, **], Wen-Shuai Zhu [a, ***]

[a] School of Chemistry and Chemical Engineering, Institute for Energy Research, Jiangsu University, Zhenjiang, Jiangsu, 212013, PR China
[b] School of Pharmacy, Jiangsu University, Zhenjiang, Jiangsu, 212013, PR China
[c] Yangzhou University, Yangzhou, Jiangsu, 225002, PR China
[d] Fine Chemical Industry Research Institute, School of Chemistry, Sun Yat-sen University, Guangzhou, Guangdong, 510275, PR China

ARTICLE INFO

Article history:
Received 31 May 2021
Accepted 13 August 2021
Available online 12 November 2021

Edited by Xiu-Qiu Peng

Keywords:
N-hydroxyphthalimide
Hexagonal boron nitride
Oxidative desulfurization
Heterogeneous catalysis

ABSTRACT

A metal-free N-hydroxyphthalimide/hexagonal boron nitride (NHPI/h-BN) catalytic system was developed for deep oxidative desulfurization (ODS) of fuel oils. Detailed experiments find that the heterogenization process of loading NHPI on h-BN not only benefits to the dispersion and utilization of NHPI, but also can significantly promote the catalytic performance. By employing NHPI/h-BN as the catalyst, azodiisobutyronitrile (AIBN) as the metal-free initiator, a 95% conversion of dibenzothiophene (DBT) can be acquired under the reaction conditions of 120 °C and atmospheric pressure with molecular oxygen (O_2) as oxidant. Moreover, the heterogenization is convenient for the regeneration of the catalyst with >94% DBT conversion after being recycled seven times. Characterizations illustrate that the promoted catalytic activity along with the regenerability originate from the interactions between NHPI and h-BN. The catalytic mechanism study shows that molecular oxygen is readily activated by the NHPI/h-BN to form a superoxide radical ($O_2^{\bullet-}$), which oxidize DBT to $DBTO_2$ for desulfurization.

1. Introduction

Recently, environmental pollution has emerged to be a major global problem because of the massive use of fossil fuels. The combustion of sulfur-containing compounds in fuels is the major cause of air pollution (Khan et al., 2020). Thusly, the clean utilization of fuel oils has turned to be an urgent demand. Currently, hydrodesulfurization (HDS) is the predominant technology for the remove of sulfides in the industry which requires high temperature (>300 °C) and pressure (>3.0 MPa) (Astle et al., 2019; Hajjar et al., 2018; Wang et al., 2020). Inevitably, the harsh conditions will result in large energy consumption. Meanwhile, the remove of aromatic sulfides, especially 4,6-dimethylbenzothiophenes (4,6-DMDBT), by HDS moderately is still a challenge. So far, several alternative desulfurization methods have been studied as a supplement to HDS for the removal of aromatic sulfides under moderate condition such as extractive desulfurization (EDS) (Lee et al., 2020; Li et al., 2013; Zhu et al., 2020), adsorptive desulfurization (ADS) (Kabtamu et al., 2020; Luo et al., 2021; Shi et al., 2020), biodesulfurization (BDS) (Silva et al., 2020; Sousa et al., 2020; Tatangelo et al., 2016) and oxidative desulfurization (ODS) (Ghubayra et al., 2019; Kampouraki et al., 2019; Yao et al., 2019).

Among them, ODS has drawn much attentions because of its low capital investment and high catalytic efficiency to the refractory aromatic compounds. In the ODS technology, the sulfides will be oxidized to the sulfoxides or sulfones with increased polarity under the assistance of oxidant and catalyst, and the oxidation product can be easily separated from the fuels by extraction, and adsorption (Luo et al., 2019; Zou et al., 2021). More recently, Kang et al. (2018) had reported using the filtration method to separate the sulfone, which was simpler and more effective.

Nowadays, various kinds of oxidants have been applied into the ODS process, for example, ozone (O_3) (Ma et al., 2014), hydrogen peroxide (H_2O_2) (Jiang et al., 2019), organic hydroperoxides (Chang

* Corresponding author.
** Corresponding author.
*** Corresponding author.
E-mail addresses: wupeiwen@ujs.edu.cn (P.-W. Wu), jihb@mail.sysu.edu.cn (H.-B. Ji), zhuws@ujs.edu.cn (W.-S. Zhu).

https://doi.org/10.1016/j.petsci.2021.11.010

et al., 2020; Smolders et al., 2019) and molecular oxygen (O_2) (Dong et al., 2019; Song et al., 2019). And the O_2 is an ideal one because of its low price and environmentally friendly characteristics. Nevertheless, it is difficult to be activated due to its high activation barrier (Zhang et al., 2012). Therefore, the seeking of an appropriate catalyst to activate O_2 efficiently is the central topic of this work.

N-hydroxyphthalimide (NHPI) has lately shown notable performances in the aerobic catalysis of multiple organic compounds under moderate conditions by a free-radical chain mechanism, among them the NHPI is converted to phthalimido-N-oxyl (PINO) radical in situ under the aerobic condition to advance the reaction. The process can be accelerated in the presence of an initiator, such as transition metals salts, especially Co^{2+} ions salts (Arzumanyan et al., 2018; Hruszkewycz et al., 2017; Ma et al., 2019; Mahmood et al., 2018). Despite the high efficiency of NHPI, its further application in an industrial scale is hindered due to the difficulty in recovering from the reaction system. What's more, the generated PINO radical is unstable and will decompose under aerobic conditions (Rajabi and Karimi, 2005).

To overcome this issue, many researchers have reported the strategy of immobilize NHPI on certain supports. Blandez et al. (2018) reported a heterogeneous catalyst in which NHPI anchored on diamond nanoparticles (DH) and was applied to the selective oxidation of benzylic hydrocarbons and cyclic alkenes. The NHPI/DH catalyst can be recycled three times with the minimum turnover number of 20600. Dhakshinamoorthy et al. (2012) loaded the NHPI onto the metal-organic framework (MOF) material for catalyzing cycloalkenes aerobic oxidation. It was found that there was only a slight decrease in the conversion of cyclooctene oxidation after two reuses. Hence, it can be efficient to find a proper support to heterogenization the NHPI for boosting catalytic activity and regeneration.

Up to now, various materials including titanium dioxide (TiO_2), mesoporous silica (SiO_2), magnesium oxide (MgO) and MOFs (Chen et al., 2020; Khan et al., 2014; Wang et al., 2021; Xun et al., 2016; Zeng et al., 2020) etc. have been widely investigated as supports. Although it promotes the separation, the introduction of these supports also brings a lot of shortages. For example, the MgO with low specific surface areas (SSAs) is unable to achieve the effective dispersion of active centers. The pore structure of SiO_2 with high SSAs would be clogged and aggregated during the reaction process, resulting in a decrease in catalytic activity. Additionally, the synthesis of MOFs is relatively complicated, which is an obstacle for their further applications. Recently, the newly developed two-dimensional hexagonal boron nitride (h-BN) material, an analogues of graphene, has achieved great attention because of its high SSAs, high thermal stability and good chemical inertness, which is suitable for use as support under aerobic oxidative conditions (Wu et al. 2017, 2020; Zhu et al., 2014).

Herein, we explored an NHPI/h-BN-catalyzed oxidative desulfurization system. The catalyst was synthesized via the facile impregnation method. The heterogenization process of loading NHPI on h-BN can achieve an effective dispersion of active centers, thereby improving the desulfurization performance of 95% within 6 h with a proper loading amount. During the reaction, the azodiisobutyronitrile (AIBN) was used as an initiator instead of the traditional metal salts to prevent secondary metal pollution to fuel oils. Additionally, the prepared heterogeneous catalyst is facilitated for the regeneration procedure after ODS reaction.

2. Experimental

2.1. Materials

N-hydroxyphthalimide (NHPI, 98%) and dodecane ($C_{12}H_{26}$, 98%) were obtained from Shanghai Macklin Biochemical Co., Ltd. Azodiisobutyronitrile (AIBN, 99%) and hexadecane ($C_{16}H_{34}$, AR) were obtained from Aladdin industrial corporation. Methylene chloride (CH_2Cl_2, AR) was obtained from Shanghai Sinopharm Chemical Reagent Co., Ltd. 4-Methyldibenzothiophene (4-MDBT, 97%), dibenzothiophene (DBT, 98%), 4,6-dimethydibenzothiophene (4,6-DMDBT, 97%), and hexagonal boron nitride (h-BN, 98%) were obtained from Sigma-Aldrich.

2.2. Characterizations

Scanning electron microscopy (SEM) was recorded on a JSM-6010PLUS/LA electron microscope. X-ray powder diffraction (XRD) patterns were measured by a XRD-6100 Lab (Shimadzu, Japan) with Cu-Kα radiation ($\lambda = 1.5406$ Å) at a scanning rate of 7° min^{-1}. Fourier transform infrared (FT-IR) spectra were operated by a Nicolet iS50 FT-IR spectrometer using KBr as diluents. The solid state ^1H MAS NMR spectra were acquired from a AVANCE III 400 MHz nuclear magnetic resonance spectrometer (Bruker, Germany).

2.3. Synthesis of samples

A certain mass of commercial-grade NHPI was first dispersed in 10 mL of ethanol under 60 °C. Subsequently, the commercial-grade h-BN was added in at a certain mass ratio, and then condensed and refluxed at 60 °C for 7 h. After removing most of the solvent by rotary evaporation, it was dried at 60 °C to obtain a catalyst with a different NHPI loading. The samples were denoted as NHPI/h-BN-x, where x (25, 30, 35) represented the mass fraction of NHPI in the catalysts.

2.4. Examination of ODS performance

The model fuels with an initial S-content of 200 ppm were prepared by dissolving different aromatic sulfides in dodecane, respectively, in which 4000 ppm of hexadecane was added as internal standard.

In the catalytic oxidative reaction, catalyst (50 mg) and model fuel (20 mL) were dumped into a 50 mL three-necked flask. Simultaneously, 10 mg of AIBN was added as an initiator and carried out under 120 °C with vigorously stirred, and the air from the atmosphere was continuously blew into the system with 100 mL min^{-1}. After reaction for a certain time, the upper oil phase was taken out and analyzed by a gas chromatograph (GC, Agilent-7890A), which was equipped with a flame ionization detector (FID) and a HP-5 type column (30 m × 0.32 mm × 0.25 μm). The sulfur conversion was used to evaluate the efficiency of sulfide being oxidized to the corresponding sulfone and calculated through the following formula:

$$Sulfur\ conversion\ (\%) = \frac{C_0 - C_t}{C_0} \times 100\%$$

where the C_0 referred to the initial S-concentration and the C_t referred to the S-concentration after reacting for t h.

After the reaction, the oxidation products were determined via a gas chromatography-mass spectrometry (GC-MS, Agilent 7890A-5975) with the following program. GC injector temperature: 200 °C. Oven: heating from 100 °C to 200 °C with a rate of 15 °C min^{-1}, holding for 1 min, and then raising to 240 °C with 10 °C min^{-1}. Column type: HP-5 (30 m × 0.32 mm × 0.25 μm). MS adopts EI mode with the ion source temperature of 230 °C.

During the real oil oxidation reaction, 100 mg of NHPI/h-BN-30 and 20 mg of AIBN were added to the reaction equipped with 40 mL of real oil with the air rate of 100 mL min^{-1}. The sulfur content was detected by the ultraviolet fluorescence sulfur meter (GCTS-3000).

3. Results and discussion

Firstly, SEM was carried out to directly investigate the morphology of sample (Fig. 1), in which the NHPI/h-BN-30 catalyst exhibited a typical two-dimensional graphene-like structure of h-BN (Wu et al., 2020), indicating that the morphology of the catalyst has no change after immobilizing NHPI. Meanwhile, the corresponding elemental mapping images showed that all of the elements of N, O, C were uniformly dispersed on the h-BN surface (Fig. 1b), suggesting the fine dispersion of NHPI after the heterogenization process.

The detailed structure of the synthesized catalyst was further determined by XRD (Fig. 2a). The diffraction peaks in the XRD pattern of NHPI/h-BN-30 centered at 25.6° and 41.6° were attributed to the (002) and (100) planes, respectively, which consistent with the hexagonal arrangement of h-BN (Zhu et al., 2016). Besides, the characteristic peaks of NHPI can also be detected in NHPI/h-BN-30, indicating that NHPI has been successfully loaded onto h-BN.

The strong absorption peaks at 818 cm^{-1} and 1397 cm^{-1} in FT-IR spectra (Fig. 2b) were attributed to the out-of-plane bending vibration and in-plane stretching vibration of B—N bond, respectively (Chen et al., 2018). Importantly, the weaker peaks at 1703 cm^{-1} and 699 cm^{-1} can be assigned to the characteristic peaks of benzene ring in NHPI and no shift of the peaks occurred. All of these characterizations confirmed the successful preparation of the heterogeneous NHPI/h-BN catalyst and the structure of h-BN were largely maintained.

In the ^{1}H MAS NMR patterns (Fig. 3), the chemical shift at 6.006 ppm of NHPI shifted to the high field (6.288 ppm) after being immobilized onto h-BN, indicating the change of chemical environment of H atom in NHPI. Additionally, a new split peak can be observed at 0.610 ppm, owing to the deviation of the H atom in NHPI, suggesting the formation of a chemical interaction between NHPI and h-BN, which will be beneficial for the stability of the catalyst.

4. Investigation of catalytic activity of catalysts

The effect of different NHPI loading amounts on ODS was firstly examined in Fig. 4. The catalytic activity with different loading amounts of 25%, 30%, and 35% was investigated respectively. It can be observed that the catalyst with a 30% loading amount had the best catalytic activity of 95% DBT conversion within 6 h under 120 °C. When the loading amount increased to 35%, the desulfurization performance dropped obviously to 56%, which was owing to the agglomeration of the active center. Therefore, the catalyst of NHPI/h-BN-30 with a loading amount of 30% was selected as the optimum one for the subsequent studies.

Subsequently, different desulfurization experiments were carried out to assess the effect of the heterogenization process. Interestingly, the catalytic performance of NHPI/h-BN-30 was improved to 95% after heterogenization, compared to the 55% DBT conversion of pristine NHPI (Fig. 5, curves c and d), and the 20% DBT conversion of commercial bulk h-BN (curve b). Similarly, the catalytic activity of the physical mixture of NHPI and h-BN was only 57% (curve e). This indicated that the loading of NHPI was favorable for dispersing the active site, thereby improving the desulfurization performance. What's more, the performance of NHPI/h-BN-30 was also studied without the addition of AIBN (curve a) and the DBT conversion decreased sharply to 48%, suggesting the important role of AIBN as an initiator to promote the generation of radicals.

To confirm the superior ODS catalytic performance of this work, the comparison of catalytic activity on different catalysts with h-BN as support was listed in Table 1. Most of the catalytic systems used metal-base material as the active center, which to a certain extend increased the investment during the practical industry application. Meanwhile, the metal-free system can effectively prevent secondary metal pollution in oil. Furthermore, compared to the Pt/h-BN catalyst (entries 1 and 2), the reaction temperature of this work was lower, which was beneficial to reduce the energy consumption. And in terms of the catalyst usage amount, the amount of this system was also relatively small. In summary, this work shows better catalytic performance than previously reported ones.

Moreover, the desulfurization performance of different substrates was investigated in Fig. 6a and the conversion of DBT, 4,6-DMDBT, and 4-MDBT were 97%, 95%, and 62%, respectively, after 8 h. The difference in the catalytic activity was mainly related to the $f^{-}(r)$ Fukui function, which indicated the sensitivity of sulfur atoms to the electrophilic attacks (Li et al., 2016). The $f^{-}(r)$ values of different sulfides were 0.331 (DBT), 0.292 (4-MDBT), and 0.304 (4,6-DMDBT), respectively. Generally, the value of $f^{-}(r)$ is positively correlated with catalytic activity, so the 4-MDBT exhibits the lowest reactivity. Besides, it is worth noting that a deep desulfurization (residual S-content < 10 ppm) of 4,6-DMDBT, which is considered to be the refractory sulfide in the HDS technology, can be achieved, suggesting the superiority of this catalyst.

In addition, fluid catalytic cracking (FCC) diesel was selected as the representative real oil to examine the efficiency of NHPI/h-BN-30 in real oil. The initial sulfur content of real oil was 554 ppm and decreased to 446 ppm after extraction once by acetonitrile.

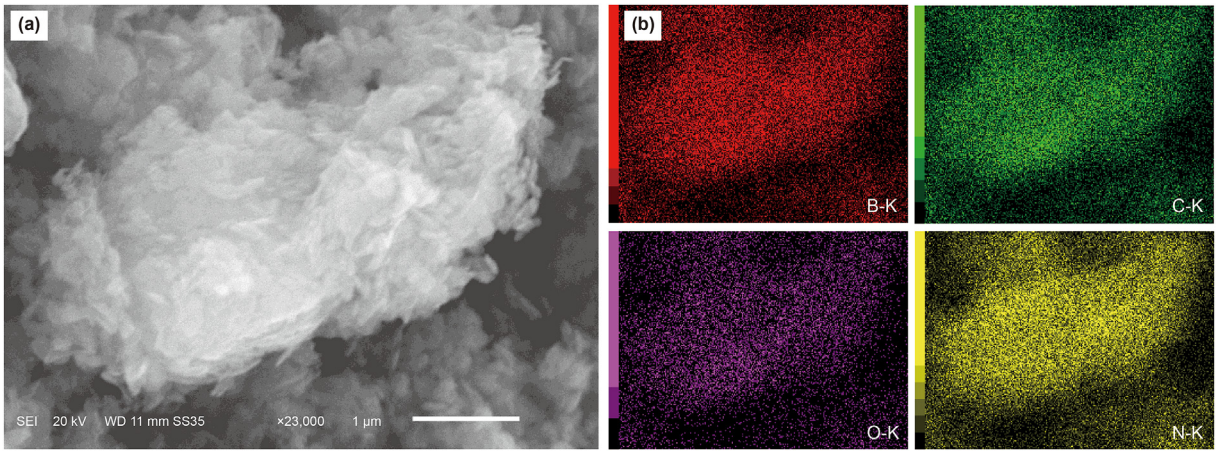

Fig. 1. (a) SEM image of NHPI/h-BN-30; (b) Elemental mapping images of NHPI/h-BN-30.

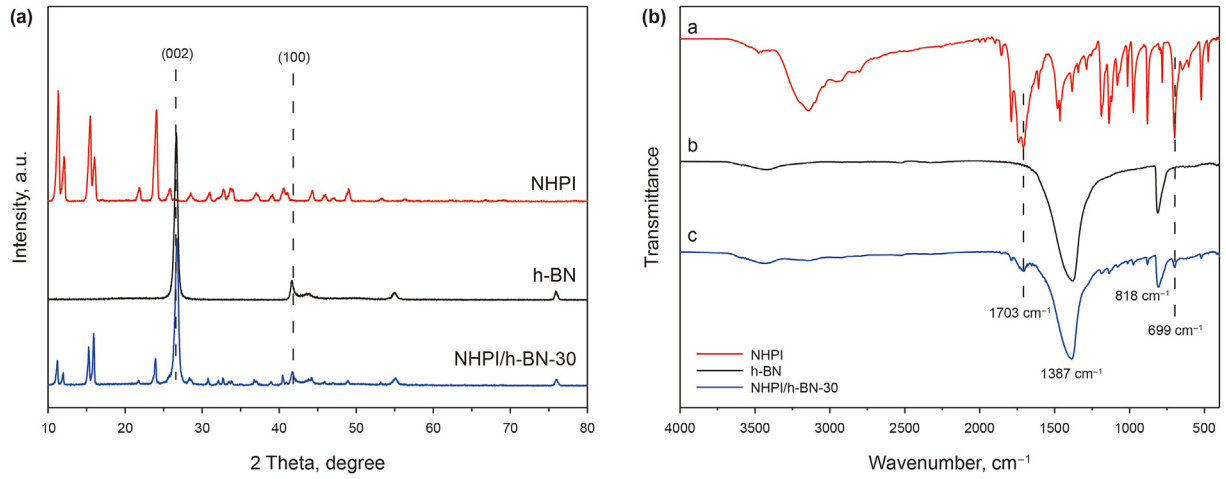

Fig. 2. (a) XRD patterns and (b) FT-IR spectra of NHPI, h-BN and NHPI/h-BN-30.

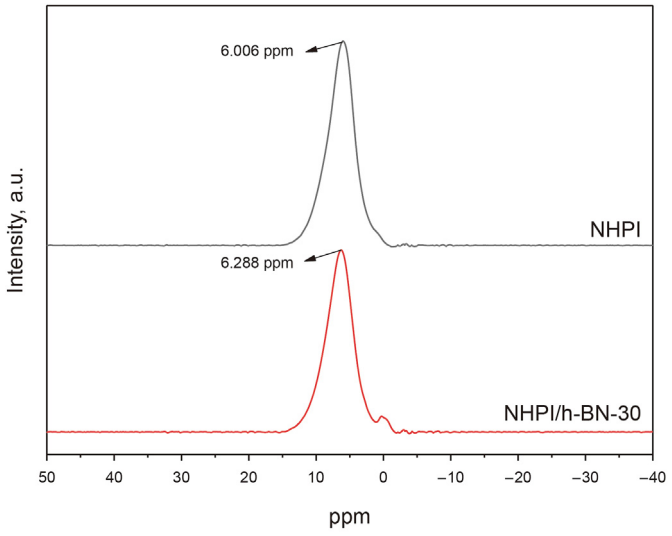

Fig. 3. ^{1}H MAS NMR patterns of NHPI and NHPI/h-BN-30.

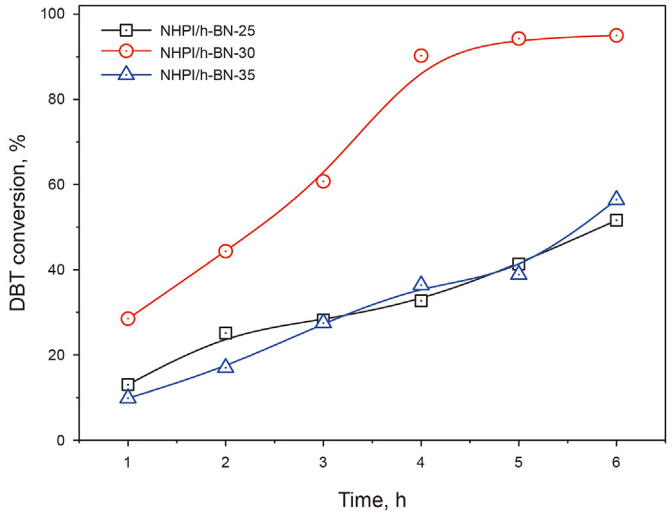

Fig. 4. Effect of the NHPI loading amount on the DBT conversion. Experiment conditions: *m* (NHPI/h-BN) = 50 mg, *m* (AIBN) = 10 mg, *V* (model fuel) = 20 mL, *T* = 120 °C.

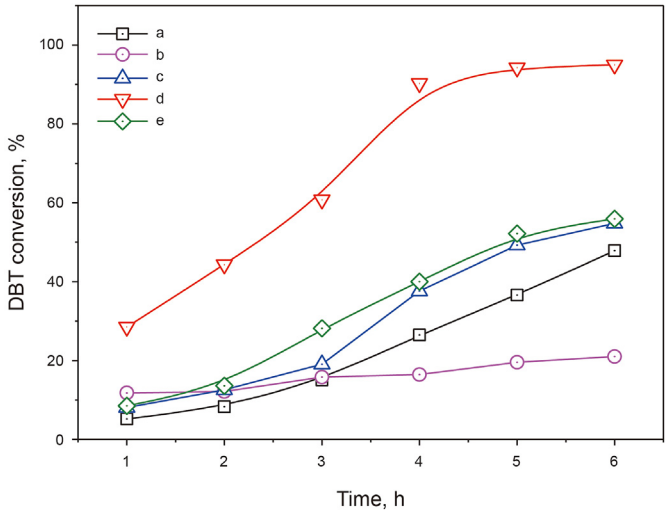

Fig. 5. Catalytic performance of different desulfurization systems. Experiment conditions: *m* (catalyst) = 50 mg, *m* (AIBN) = 10 mg, *V* (model fuel) = 20 mL, *T* = 120 °C. a. NHPI/h-BN-30; b. h-BN + AIBN; c. NHPI + AIBN; d. NHPI/h-BN-30+AIBN; e. NHPI + h-BN + AIBN

Similarly, the reacted oil was extracted by acetonitrile for once to remove the produced sulfone. The result was showed in Fig. 6b. After reaction for 8 h, the residual S-content in real oil dropped sharply to 123 ppm with the sulfur removal of 78%. The presence of aromatic hydrocarbons and olefins in real oil may affect the catalytic performance to some extent (He et al., 2021).

To deeply understand the oxidation process, the GC-MS was performed to determine the oxidation product (Fig. 7). The upper oil phase was measured by GC-MS directly. The solid catalyst was extracted by CH_2Cl_2 and the extraction phase was collected for detection. The main species in the oil phase was DBT (m/z = 184.0), and in the solid catalyst phase, only the $DBTO_2$ (m/z = 216.0) signal can be observed, which suggested that the $DBTO_2$ was the only oxidation product and will be absorbed onto the catalyst surface (Xun et al., 2020). It is conducive to the removal of sulfides with the separation of catalysts.

The ESR characterization was then carried out to further investigate the active intermediate during the reaction. As shown in Fig. 8 that there was no ESR signal in the absence of NHPI/h-BN-30 or O_2, which proved that the catalyst and oxidant were

Table 1
Comparison of ODS performance on different h-BN based catalysts*.

Entry	Catalyst	*T*, °C	*m*, mg	S conversion, %	Reference
1	Pt/h-BN	130	50	98	Wu et al. (2020)
2	Pt/h-BN	120	50	62	Wu et al. (2020)
3	5-MoO_xNPs/g-BN	120	100	100	Yao et al. (2019)
4	10 wt% V_2O_5/BNNS	120	200	99	Wang et al. (2020)
5	PtCu/BNNS	110	80	96	He et al. (2020)
6	$[C_8mim]_3H_3V_{10}O_{28}$/g-BN	120	80	99	Wang et al. (2018)
7	NHPI/h-BN-30	120	50	95	This work

*Oxidant: air.

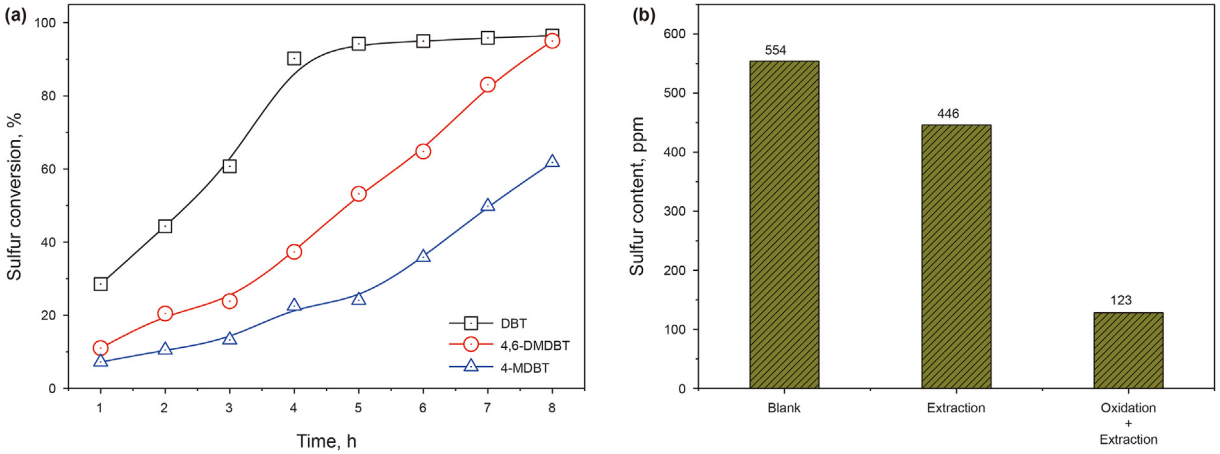

Fig. 6. (a) Catalytic performance of different substrates; (b) Desulfurization efficiency of NHPI/h-BN-30 to real oil. Experiment conditions: (a) *m* (NHPI/h-BN-30) = 50 mg, *m* (AIBN) = 10 mg, *V* (model fuel) = 20 mL, *T* = 120 °C; (b) *m* (NHPI/h-BN-30) = 100 mg, *m* (AIBN) = 20 mg, *V* (FCC diesel) = 40 mL, *T* = 120 °C.

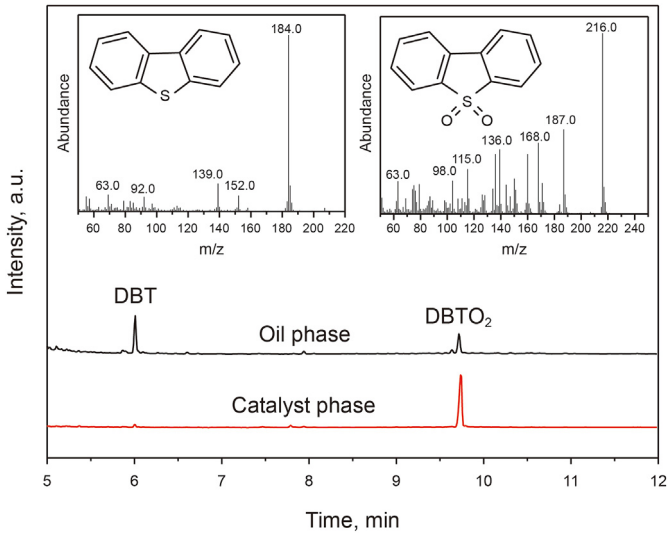

Fig. 7. Detection of oxidation product by GC-MS.

indispensable for the generation of free radicals. With the introduction of O_2, there was a signal which attributed to the superoxide radical ($O_2^{\bullet-}$). Meanwhile, with the addition of AIBN, the intensity of the signal increased significantly, indicating that the presence of AIBN can indeed promote the generation of free radicals which was consistent with the experimental results of Fig. 5. At the same time, the selective quenching experiments were performed to further determine the active oxygen species, in which BQ or TBA was used as the quenchers of $O_2^{\bullet-}$ or hydroxyl radicals (HO•), respectively. The catalytic performance did not changed after the addition of TBA, whereas the injection of BQ inhibited the ODS performance greatly, demonstrating the presence of $O_2^{\bullet-}$ radicals.

Hence, a mechanism can be raised based on the above results. Firstly, the NHPI was converted to PINO in situ under the oxidative condition and subsequently activated the O_2 to $O_2^{\bullet-}$ radicals. At the same time, the DBT turned to sulfur-centered cation radical (Gu et al., 2017) and reacted with the $O_2^{\bullet-}$ radicals to generate the corresponding sulfones species (Fig. 9). After that, the oxidation products will adsorb onto the catalyst surface, thus can realize the removal of sulfides with the separation of the catalyst. During this process, the presence of AIBN can accelerate the generation of PINO radicals and promote the activation of O_2.

5. Regeneration performance

The regeneration of the catalyst after the ODS process was performed as follows: Firstly, after standing a while, most of the model fuel was removed from the reaction system through decantation, followed by centrifugation to remove the remaining model fuel. The catalyst was then dried for the next reaction. After being recycled three times, the desulfurization efficiency slightly dropped to 92%, which resulted from the accumulation of sulfone on the catalyst surface and it was raised to 95% by washing with CH_2Cl_2 to remove the sulfone. And a deep DBT conversion of 94% can still be achieved after being recycled seven times (Fig. 10).

The FT-IR and XRD characterizations of the used catalyst were performed in Fig. 11 to confirm the structure change before and after the reaction. In the FT-IR (Fig. 11a), the characteristic

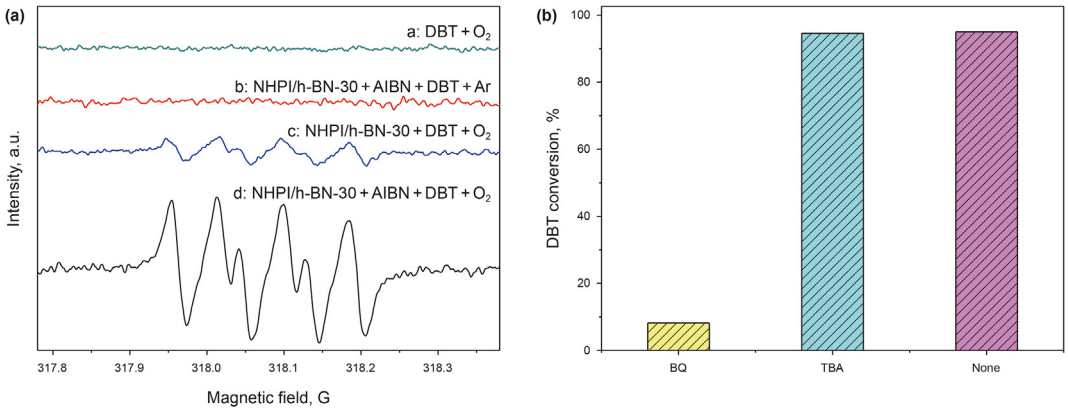

Fig. 8. (a) ESR spectra of the NHPI/h-BN-30 system; (b) Selective quenching experiments.

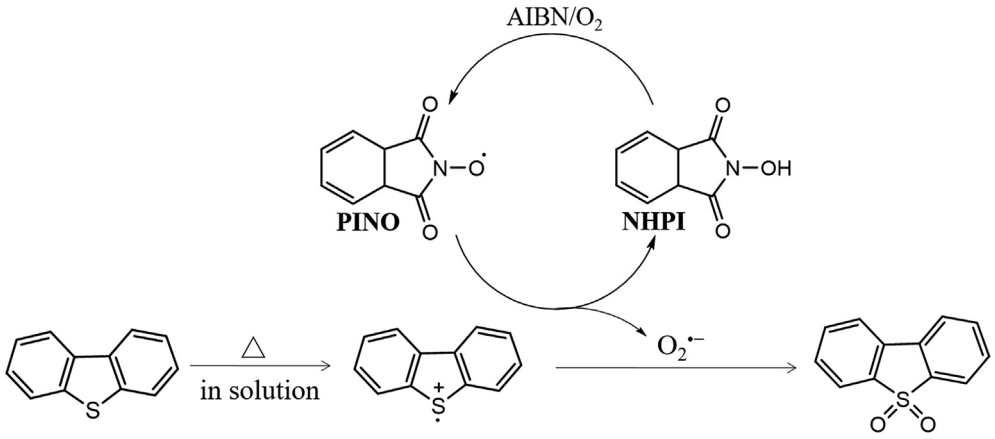

Fig. 9. The reaction mechanism of catalytic oxidation of DBT.

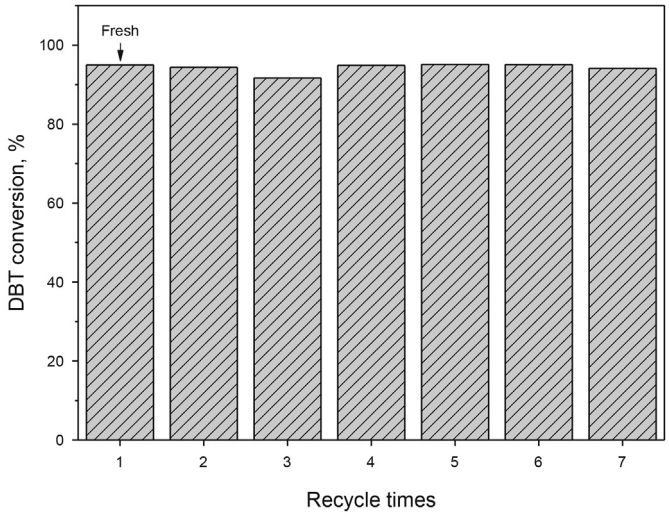

Fig. 10. Regeneration performance of NHPI/h-BN-30.

absorption peaks of NHPI/h-BN-30 can still be detected, indicating the structural stability of the sample. And new adsorption peaks around 1164 cm^{-1} and 1284 cm^{-1} can be obtained in the used catalyst, which resulted from the S=O symmetric and asymmetric vibration, respectively, confirming the presence of $DBTO_2$ adsorbed on the catalyst surface (Nisar et al., 2011). Similarly, no change can be observed in the diffraction peaks of NHPI/h-BN-30 before and after the reaction. And the new diffraction peaks in the used catalyst can be ascribed to the $DBTO_2$ (Fig. 11b). In general, the catalyst was stable during the ODS reaction with oxidation product adsorbed on the catalyst.

6. Conclusions

In summary, a heterogeneous metal-free catalyst was synthesized by a simple impregnation method successfully with commercially available NHPI anchored on h-BN. The NHPI/h-BN catalyst is highly effective for the oxidation of aromatic sulfides with 95% conversion of DBT using metal-free AIBN as the initiator at 120 °C. GC-MS proved the fully selective conversion of DBT to the sulfone of $DBTO_2$. Based on the serious characterizations, a reasonable mechanism can be proposed that the O_2 was activated to the $O_2^{\bullet-}$ radicals by NHPI after it converted to PINO radicals with the assistance of AIBN, subsequently, oxidized the sulfides to the sulfones and adsorbed onto the catalyst surface. Additionally, the regenerability of the catalyst was confirmed with a 94% DBT conversion after being recycled seven times.

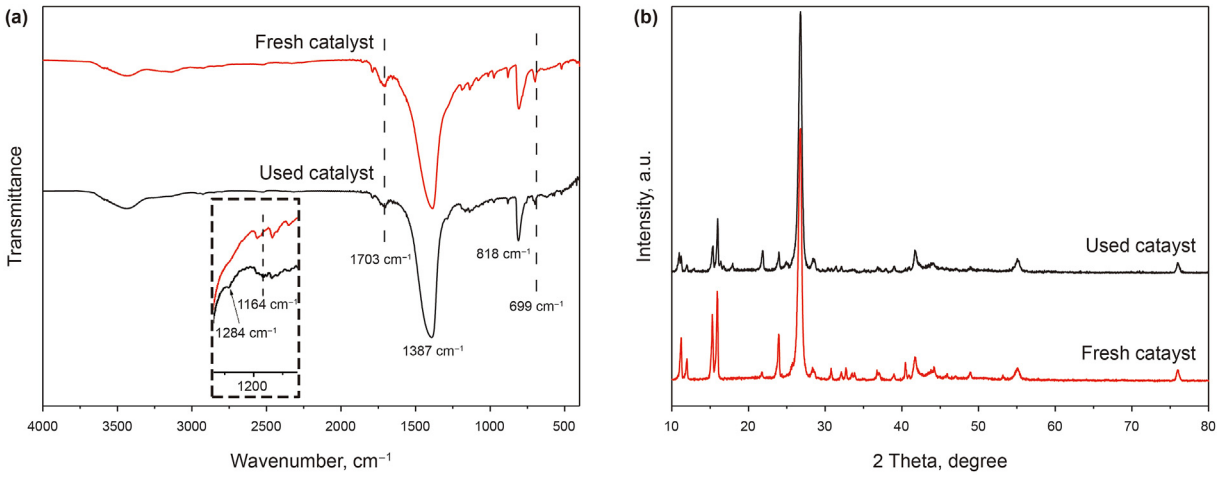

Fig. 11. FT-IR spectra and XRD patterns of NHPI/h-BN-30 before and after reaction.

Acknowledgements

All authors appreciate the financial support from the National Key R&D Program of China (No. 2017YFB0306504), National Natural Science Foundation of China (No. 22008094, 22178154 and 21878133), Chinese Postdoctoral Science Foundation (No. 2019M651743, 2020M671364 and 2020M673039), Natural Science Foundation of Jiangsu Province (No. BK20190852), Natural Science Foundation for Jiangsu Colleges and Universities (No. 19KJB530005).

References

Arzumanyan, A.V., Goncharova, I.K., Novikov, R.A., Milenin, S.A., Boldyrev, K.L., Solyev, P.N., Tkachev, Y.V., Volodin, A.D., Smol'yakov, A.F., Korlyukov, A.A., Muzafarov, A.M., 2018. Aerobic Co or Cu/NHPI-catalyzed oxidation of hydride siloxanes: synthesis of siloxanols. Green Chem. 20 (7), 1467–1471. https://doi.org/10.1039/C8GC00424B.

Astle, M.A., Rance, G.A., Loughlin, H.J., Peters, T.D., Khlobystov, A.N., 2019. Molybdenum dioxide in carbon nanoreactors as a catalytic nanosponge for the efficient desulfurization of liquid fuels. Adv. Funct. Mater. 29 (17), 1808092. https://doi.org/10.1002/adfm.201808092.

Blandez, J.F., Navalón, S., Álvaro, M., García, H., 2018. N-hydroxyphthalimide anchored on diamond nanoparticles as a selective heterogeneous metal-free oxidation catalyst of benzylic hydrocarbons and cyclic alkenes by molecular O_2. ChemCatChem 10 (1), 198–205. https://doi.org/10.1002/cctc.201700886.

Chang, X., Yang, X.F., Qiao, Y., Wang, S., Zhang, M.H., Xu, J., Wang, D.H., Bu, X.H., 2020. Confined heteropoly blues in defected Zr-MOF (bottle around ship) for high-efficiency oxidative desulfurization. Small 16 (4), e1906432. https://doi.org/10.1002/smll.201906432.

Chen, J., Zhang, M.S., Pang, C., Xiang, F.W., Zhu, M.J., Ma, X.C., Chang, G.G., Yin, W.Y., 2020. Hydrophilic Pd/MgO nanosystem for the highly efficient aqueous-phase catalysis of suzuki-Miyaura reactions. Ind. Eng. Chem. Res. 59 (1), 81–87. https://doi.org/10.1021/acs.iecr.9b05248.

Chen, S.R., Li, P., Xu, S.T., Pan, X.L., Fu, Q., Bao, X.H., 2018. Carbon doping of hexagonal boron nitride porous materials toward CO_2 capture. J. Mater. Chem. A 6 (4), 1832–1839. https://doi.org/10.1039/c7ta08515j.

Dhakshinamoorthy, A., Alvaro, M., Garcia, H., 2012. Aerobic oxidation of cycloalkenes catalyzed by iron metal organic framework containing N-hydroxyphthalimide. J. Catal. 289, 259–265. https://doi.org/10.1016/j.jcat.2012.02.015.

Dong, Y.L., Zhang, J.H., Ma, Z.H., Xu, H., Yang, H.W., Yang, L.X., Bai, L.J., Wei, D.L., Wang, W.X., Chen, H., 2019. Preparation of Co-Mo-O ultrathin nanosheets with outstanding catalytic performance in aerobic oxidative desulfurization. Chem. Commun. 55 (93), 13995–13998. https://doi.org/10.1039/c9cc07452j.

Ghubayra, R., Nuttall, C., Hodgkiss, S., Craven, M., Kozhevnikova, E.F., Kozhevnikov, I.V., 2019. Oxidative desulfurization of model diesel fuel catalyzed by carbon-supported heteropoly acids. Appl. Catal. B Environ. 253, 309–316. https://doi.org/10.1016/j.apcatb.2019.04.063.

Gu, Q.Q., Wen, G.D., Ding, Y.X., Wu, K.H., Chen, C.M., Su, D.S., 2017. Reduced graphene oxide: a metal-free catalyst for aerobic oxidative desulfurization. Green Chem. 19 (4), 1175–1181. https://doi.org/10.1039/C6GC02894B.

Hajjar, Z., Kazemeini, M., Rashidi, A., Soltanali, S., 2018. Hydrodesulfurization catalysts based on carbon nanostructures: a review. Fullerenes, Nanotub. Carbon Nanostruct. 26 (9), 557–569. https://doi.org/10.1080/1536383x.2018.1470509.

He, J., Wu, P., Chen, L., Li, H., Hua, M., Lu, L., Wei, Y., Chao, Y., Zhou, S., Zhu, W., Li, H., 2021. Dynamically-generated TiO_2 active site on MXene Ti_3C_2: boosting reactive desulfurization. Chem. Eng. J. 416, 129022. https://doi.org/10.1016/j.cej.2021.129022.

He, J., Wu, Y., Wu, P., Lu, L., Deng, C., Ji, H., He, M., Zhu, W., Li, H-m, 2020. Synergistic catalysis of the PtCu alloy on ultrathin BN nanosheets for accelerated oxidative desulfurization. ACS Sustain. Chem. Eng. 8 (4), 2032–2039. https://doi.org/10.1021/acssuschemeng.9b06586.

Hruszkewycz, D.P., Miles, K.C., Thiel, O.R., Stahl, S.S., 2017. Co/NHPI-mediated aerobic oxygenation of benzylic C-H bonds in pharmaceutically relevant molecules. Chem. Sci. 8 (2), 1282–1287. https://doi.org/10.1039/c6sc03831j.

Jiang, W., Jia, H., Li, H., Zhu, L., Tao, R., Zhu, W., Li, H., Dai, S., 2019. Boric acid-based ternary deep eutectic solvent for extraction and oxidative desulfurization of diesel fuel. Green Chem. 21 (11), 3074–3080. https://doi.org/10.1039/c9gc01004a.

Kabtamu, D.M., Wu, Y.N., Chen, Q., Zheng, L., Otake, K.I., Matoyic, L., Li, F., 2020. Facile upcycling of hazardous Cr-containing electroplating sludge into value-added metal-organic frameworks for efficient adsorptive desulfurization. ACS Sustain. Chem. Eng. 8 (33), 12443–12452. https://doi.org/10.1021/acssuschemeng.0c03110.

Kampouraki, Z.C., Giannakoudakis, D.A., Triantafyllidis, K.S., Deliyanni, E.A., 2019. Catalytic oxidative desulfurization of a 4,6-DMDBT containing model fuel by metal-free activated carbons: the key role of surface chemistry. Green Chem. 21 (24), 6685–6698. https://doi.org/10.1039/C9GC03234G.

Kang, L., Liu, H., He, H., Yang, C., 2018. Oxidative desulfurization of dibenzothiophene using molybdenum catalyst supported on Ti-pillared montmorillonite and separation of sulfones by filtration. Fuel 234, 1229–1237. https://doi.org/10.1016/j. fuel.2018.07.148.

Khan, N.A., Bhadra, B.N., Park, S.W., Han, Y.S., Jhung, S.H., 2020. Tungsten nitride, well-dispersed on porous carbon: remarkable catalyst, produced without addition of ammonia, for the oxidative desulfurization of liquid fuel. Small 16 (12), 1901564. https://doi.org/10.1002/smll.201901564.

Khan, N.A., Hasan, Z., Jhung, S.H., 2014. Ionic liquids supported on metal-organic frameworks: remarkable adsorbents for adsorptive desulfurization. Chem. Eur J. 20 (2), 376–380. https://doi.org/10.1002/chem.201304291.

Lee, H., Kang, S., Jin, Y., Jung, D., Park, K., Li, K., Lee, J., 2020. Systematic investigation of the extractive desulfurization of fuel using deep eutectic solvents from multifarious aspects. Fuel 264, 116848. https://doi.org/10.1016/j.fuel.2019.116848.

Li, C., Li, D., Zou, S., Li, Z., Yin, J., Wang, A., Cui, Y., Yao, Z., Zhao, Q., 2013. Extraction desulfurization process of fuels with ammonium-based deep eutectic solvents. Green Chem. 15 (10), 2793–2799. https://doi.org/10.1039/C3GC41067F.

Li, H.P., Zhu, W.S., Zhu, S.W., Xia, J.X., Chang, Y.H., Jiang, W., Zhang, M., Zhou, Y.W., Li, H.M., 2016. The selectivity for sulfur removal from oils: an insight from conceptual density functional theory. AlChE J 62 (6), 2087–2100. https://doi.org/10.1002/aic.15161.

Luo, J., Wang, C., Liu, J., Wei, Y., Chao, Y., Zou, Y., Mu, L., Huang, Y., Li, H., Zhu, W., 2021. High-performance adsorptive desulfurization by ternary hybrid boron carbon nitride aerogel. AlChE J, e17280. https://doi.org/10.1002/aic.17280.

Luo, Q., Zhou, Q., Lin, Y., Wu, S., Liu, H., Du, C., Zhong, Y., Yang, C., 2019. Fast and deep oxidative desulfurization of dibenzothiophene with catalysts of MoO_3-TiO_2@MCM-22 featuring adjustable Lewis and Brønsted acid sites. Catal. Sci. Technol. 9 (21), 6166–6179. https://doi.org/10.1039/C9CY01438A.

Ma, C., Dai, B., Liu, P., Zhou, N., Shi, A., Ban, L., Chen, H., 2014. Deep oxidative desulfurization of model fuel using ozone generated by dielectric barrier discharge plasma combined with ionic liquid extraction. J. Ind. Eng. Chem. 20 (5), 2769–2774. https://doi.org/10.1016/j.jiec.2013.11.005.

Ma, R., Chen, W., Wang, L., Yi, X., Xiao, Y., Gao, X., Zhang, J., Tang, X., Yang, C.,

Meng, X., Zheng, A., Xiao, F.S., 2019. N-oxyl radicals trapped on Zeolite surface accelerate photocatalysis. ACS Catal. 9 (11), 10448–10453. https://doi.org/10.1021/acscatal.9b03737.

Mahmood, S., Xu, B.H., Ren, T.L., Zhang, Z.B., Liu, X.M., Zhang, S.J., 2018. Cobalt/N-Hydroxyphthalimide(NHPI)-Catalyzed aerobic oxidation of hydrocarbons with ionic liquid additive. Mol. Catal. 447, 90–96. https://doi.org/10.1016/j.mcat.2018.01.006.

Nisar, A., Lu, Y., Zhuang, J., Wang, X., 2011. Polyoxometalate nanocone nanoreactors: magnetic manipulation and enhanced catalytic performance. Angew. Chem. Int. Ed. 50 (14), 3187–3192. https://doi.org/10.1002/anie.201006155.

Rajabi, F., Karimi, B., 2005. Efficient aerobic oxidation of alcohols using a novel combination N-hydroxy phthalimide (NHPI) and a recyclable heterogeneous cobalt complex. J. Mol. Catal. Chem. 232 (1), 95–99. https://doi.org/10.1016/j.molcata.2005.01.016.

Shi, S., Li, Y.X., Li, S.S., Liu, X.Q., Sun, L.B., 2020. Fabrication of Cu^{2+} sites in confined spaces for adsorptive desulfurization by series connection double-solvent strategy. Green Energy Environ. https://doi.org/10.1016/j.gee.2020.10.009.

Silva, T.P., Alves, L., Paixao, S.M., 2020. Effect of dibenzothiophene and its alkylated derivatives on coupled desulfurization and carotenoid production by Gordonia alkanivorans strain 1B. J. Environ. Manag. 270, 110825. https://doi.org/10.1016/j.jenvman.2020.110825.

Smolders, S., Willhammar, T., Krajnc, A., Sentosun, K., Wharmby, M.T., Lomachenko, K.A., Bals, S., Mali, G., Roeffaers, M.B.J., De Vos, D.E., Bueken, B., 2019. A titanium(IV)-Based metal-organic framework featuring defect-rich Ti-O sheets as an oxidative desulfurization catalyst. Angew. Chem. Int. Ed. 58 (27), 9160–9165. https://doi.org/10.1002/anie.201904347.

Song, J., Li, Y., Cao, P., Jing, X., Faheem, M., Matsuo, Y., Zhu, Y., Tian, Y., Wang, X., Zhu, G., 2019. Synergic catalysts of Polyoxometalate@Cationic porous aromatic frameworks: reciprocal modulation of both capture and conversion materials. Adv. Mater. 31 (40), e1902444. https://doi.org/10.1002/adma.201902444.

Sousa, J.P.M., Neves, R.P.P., Sousa, S.F., Ramos, M.J., Fernandes, P.A., 2020. Reaction mechanism and determinants for efficient catalysis by DszB, a key enzyme for crude oil bio-desulfurization. ACS Catal. 10 (16), 9545–9554. https://doi.org/10.1021/acscatal.0c03122.

Tatangelo, V., Mangili, I., Caracino, P., Anzano, M., Najmi, Z., Bestetti, G., Collina, E., Franzetti, A., Lasagni, M., 2016. Biological devulcanization of ground natural rubber by Gordonia desulfuricans DSM 44462(T) strain. Appl. Microbiol. Biotechnol. 100 (20), 8931–8942. https://doi.org/10.1007/s00253-016-7691-5.

Wang, C., Chen, Z., Yao, X., Chao, Y., Xun, S., Xiong, J., Fan, L., Zhu, W., Li, H., 2018. Decavanadates anchored into micropores of graphene-like boron nitride: efficient heterogeneous catalysts for aerobic oxidative desulfurization. Fuel 230, 104–112. https://doi.org/10.1016/j.fuel.2018.04.153.

Wang, C., Jiang, W., Chen, H., Zhu, L., Luo, J., Yang, W., Chen, G., Chen, Z., Zhu, W., Li, H., 2021. Pt nanoparticles encapsulated on V_2O_5 nanosheets carriers as efficient catalysts for promoted aerobic oxidative desulfurization performance. Chin. J. Catal. 42 (4), 557–562. https://doi.org/10.1016/S1872-2067(20)63685-3.

Wang, C., Qiu, Y., Wu, H., Yang, W., Zhu, Q., Chen, Z., Xun, S., Zhu, W., Li, H., 2020. Construction of 2D-2D V_2O_5/BNNS nanocomposites for improved aerobic oxidative desulfurization performance. Fuel 270, 117498. https://doi.org/10.1016/j. fuel.2020.117498.

Wang, X., Xiao, C., Alabsi, M.H., Zheng, P., Cao, Z., Mei, J., Shi, Y., Duan, A., Gao, D., Huang, K.W., Xu, C., 2020. Pt-confinement catalyst with dendritic hierarchical pores on excellent sulfur-resistance for hydrodesulfurization of dibenzothiophene and 4,6-dimethyldibenzothiophene. Green Energy Environ. https://doi.org/10.1016/j.gee.2020.10.012.

Wu, P., Wu, Y., Chen, L., He, J., Hua, M., Zhu, F., Chu, X., Xiong, J., He, M., Zhu, W., Li, H., 2020. Boosting aerobic oxidative desulfurization performance in fuel oil via strong metal-edge interactions between Pt and h-BN. Chem. Eng. J. 380, 122526. https://doi.org/10.1016/j.cej.2019.122526.

Wu, P.W., Lu, L.J., He, J., Chen, L.L., Chao, Y.H., He, M.Q., Zhu, F.X., Chu, X.Z., Li, H.M., Zhu, W.S., 2020. Hexagonal boron nitride: a metal-free catalyst for deep oxidative desulfurization of fuel oils. Green Energy Environ. 5 (2), 166–172. https://doi.org/10.1016/j.gee.2020.03.004.

Wu, P.W., Yang, S.Z., Zhu, W.S., Li, H.P., Chao, Y.H., Zhu, H.Y., Li, H.M., Dai, S., 2017. Tailoring N-terminated defective edges of porous boron nitride for enhanced aerobic catalysis. Small 13 (44), 1701857. https://doi.org/10.1002/smll.201701857.

Xun, S., Ti, Q., Jiao, Z., Wu, L., He, M., Chen, L., Zhu, L., Zhu, W., Li, H., 2020. Dispersing TiO_2 nanoparticles on graphite carbon for an enhanced catalytic oxidative desulfurization performance. Ind. Eng. Chem. Res. 59 (41), 18471–18479. https://doi.org/10.1021/acs.iecr.0c03202.

Xun, S.H., Zhu, W.S., Chang, Y.H., Li, H.P., Zhang, M., Jiang, W., Zheng, D., Qin, Y.J., Li, H.M., 2016. Synthesis of supported $SiW_{12}O_{40}$-based ionic liquid catalyst induced solvent-free oxidative deep-desulfurization of fuels. Chem. Eng. J. 288, 608–617. https://doi.org/10.1016/j.cej.2015.12.005.

Yao, X.Y., Wang, C., Liu, H., Li, H.P., Wu, P.W., Fan, L., Li, H.M., Zhu, W.S., 2019. Immobilizing highly catalytically molybdenum oxide nanoparticles on graphene-analogous BN: stable heterogeneous catalysts with enhanced aerobic oxidative desulfurization performance. Ind. Eng. Chem. Res. 58 (2), 863–871. https://doi.org/10.1021/acs.iecr.8b05088.

Zeng, Q., Huang, Y.J., Huang, L.M., Hu, L., Xiong, D.L., Zhong, H., He, Z.G., 2020. Efficient removal of hexavalent chromium in a wide pH range by composite of SiO_2 supported nano ferrous oxalate. Chem. Eng. J. 383, 123209. https://doi.org/10.1016/j. cej.2019.123209.

Zhang, P., Wang, Y., Li, H., Antonietti, M., 2012. Metal-free oxidation of sulfides by carbon nitride with visible light illumination at room temperature. Green Chem. 14 (7), 1904–1908. https://doi.org/10.1039/C2GC35148J.

Zhu, S., Cheng, H., Dai, Y., Gao, J., Jiang, X., 2020. Extractive desulfurization and denitrogenation from fuel oil by a polyether-amine-based solvent. Energy Fuel. 34 (7), 8186–8194. https://doi.org/10.1021/acs.energyfuels.0c01096.

Zhu, W.S., Dai, B.L., Wu, P.W., Chao, Y.H., Xiong, J., Xun, S.H., Li, H.P., Li, H.M., 2014. Graphene-analogue hexagonal BN supported with tungsten-based ionic liquid for oxidative desulfurization of fuels. ACS Sustain. Chem. Eng. 3 (1), 186–194. https://doi.org/10.1021/sc5006928.

Zhu, W.S., Gao, X., Li, Q., Li, H.P., Chao, Y.H., Li, M.J., Mahurin, S.M., Li, H.M., Zhu, H.Y., Dai, S., 2016. Controlled gas exfoliation of boron nitride into few-layered nanosheets. Angew. Chem. Int. Ed. 55 (36), 10766–10770. https://doi.org/10.1002/anie.201605515.

Zou, J., Lin, Y., Wu, S., Wu, M., Yang, C., 2021. Construction of bifunctional 3-D ordered mesoporous catalyst for oxidative desulfurization. Separ. Purif. Technol. 264, 118434. https://doi.org/10.1016/j.seppur.2021.118434.